Molecular Cell
Article

# Structure of the Human MutSα DNA Lesion Recognition Complex

Joshua J. Warren,[1,3] Timothy J. Pohlhaus,[1,3] Anita Changela,[1] Ravi R. Iyer,[1,2] Paul L. Modrich,[1,2] and Lorena S. Beese[1,*]
[1] Department of Biochemistry
[2] Howard Hughes Medical Institute
Duke University Medical Center, Durham, NC 27710, USA
[3] These authors contributed equally to this work.
*Correspondence: lsb@biochem.duke.edu
DOI 10.1016/j.molcel.2007.04.018

## SUMMARY

**Mismatch repair (MMR) ensures the fidelity of DNA replication, initiates the cellular response to certain classes of DNA damage, and has been implicated in the generation of immune diversity. Each of these functions depends on MutSα (MSH2•MSH6 heterodimer). Inactivation of this protein complex is responsible for tumor development in about half of known hereditary nonpolyposis colorectal cancer kindreds and also occurs in sporadic tumors in a variety of tissues. Here, we describe a series of crystal structures of human MutSα bound to different DNA substrates, each known to elicit one of the diverse biological responses of the MMR pathway. All lesions are recognized in a similar manner, indicating that diversity of MutSα-dependent responses to DNA lesions is generated in events downstream of this lesion recognition step. This study also allows rigorous mapping of cancer-causing mutations and furthermore suggests structural pathways for allosteric communication between different regions within the heterodimer.**

## INTRODUCTION

The DNA mismatch repair (MMR) pathway plays a crucial role in genome stabilization in both prokaryotes and eukaryotes. Inactivation of the pathway leads to replication and recombination errors. Mammals with MMR defects also fail to respond normally to certain types of DNA damage and exhibit less complex mutational patterns during the somatic hypermutation phase of B cell maturation (Iyer et al., 2006; Kunkel and Erie, 2005). Defects in human MMR are the cause of hereditary nonpolyposis colorectal cancer (HNPCC) (Kolodner, 1995) and are observed in 15%–25% of sporadic tumors in a variety of tissues (Peltomaki, 2003).

About half of HNPCC causative mutations have been localized to two genes that encode the MSH2 and MSH6 subunits of the 260 kDa MutSα complex (Peltomaki, 2003). The MutSα heterodimer recognizes mispairs and insertion/deletion loops and recruits additional factors, leading to excision of the DNA strand containing the error. A nick up to 1000 base pairs away is sufficient to direct excision to the nicked strand (Iyer et al., 2006; Jiricny, 2006; Kunkel and Erie, 2005). In addition to mismatched base pairs, MutSα recognizes certain types of DNA damage produced by chemotherapeutic agents, including $O^6$-methyl-guanine and cisplatin adducts. Recognition and perhaps processing of such lesions by the MMR system are involved in initiating checkpoint and apoptotic responses to these and several other classes of DNA damage (Iyer et al., 2006; Jiricny, 2006; Kunkel and Erie, 2005). MutSα also contributes to generation of immune diversity during class switch recombination and somatic hypermutation of B cells, an effect that has been postulated to reflect MutSα recognition of G•U mispairs produced by enzymatic deamination of cytosine (Iyer et al., 2006; Jiricny, 2006; Kunkel and Erie, 2005; Rada et al., 1998; Samaranayake et al., 2006). MutSα therefore functions as a sensor of genetic damage, the recognition or processing of which may have distinct biological outcomes (Iyer et al., 2006; Jiricny, 2006; Kat et al., 1993; Kunkel and Erie, 2005; Rada et al., 1998; Wilson et al., 2005). These context-dependent responses may indicate that MutSα responds in structurally distinct ways to different classes of base pair anomaly (Yoshioka et al., 2006). Alternatively, MutSα may utilize a common recognition mechanism for distinct lesions, with differing biological outcomes dictated by the context-dependent recruitment of downstream activities.

In addition to its DNA recognition activities, MutSα also hydrolyzes ATP (Iyer et al., 2006; Jiricny, 2006; Kunkel and Erie, 2005). MutSα contains two nonequivalent, essential ATP hydrolytic centers, located at the C termini of MSH2 and MSH6, which are members of the *A*TP *b*inding *c*assette (ABC)-transporter superfamily (Locher, 2004). Although the molecular details of MutSα function are not yet understood, it is clear that conformational coupling between DNA recognition and the nucleotide binding sites

plays a central role (Iyer et al., 2006; Jiricny, 2006; Kunkel and Erie, 2005). DNA substrate binding is known to modulate ATPase activity; conversely, ATP binding modulates DNA substrate binding: challenging complexes of MutSα and mispaired DNA with ATP leads to dissociation of MutSα from the mispair and movement along the helix contour. ATPase mutants of yeast MutSα that are defective in this response to ATP challenge (Kijas et al., 2003) act as dominant-negative inhibitors of mismatch repair (Drotschmann et al., 2004; Studamire et al., 1998). The mechanism by which MutSα transmits information between the DNA lesion and nick remains a matter of controversy (Iyer et al., 2006; Jiricny, 2006; Kunkel and Erie, 2005).

Structures of homodimeric prokaryotic MutS provided insight into features of mismatch recognition (Lamers et al., 2000; Obmolova et al., 2000), but prokaryotic MutS proteins share only limited sequence identity with human MutSα. *E. coli* MutS is only 21% and 24% identical to conserved regions of MSH2 and MSH6, respectively, and the MutS homodimer is about 600 amino acids smaller than MutSα. The low homology limits the use of prokaryotic structures to model effects of human cancer-causing mutations. Furthermore, eukaryotic MutSα is involved in pathways that prokaryotes lack: activation of programmed cell death and generation of immune diversity.

Here, we present structural information that permits alternative hypotheses about the roles of MutSα in diverse pathways to be evaluated. We have determined a series of structures of human MutSα in complex with a series of DNA substrates known to elicit different biological responses: duplex DNA with a mispair or a central unpaired nucleotide, both of which are substrates for MutSα-dependent mismatch repair; a duplex containing an $O^6$-methyl-guanine•T pair, a lesion that triggers damage signaling; and DNA containing a G•U mispair, a putative intermediate in somatic hypermutation. We find that MutSα recognizes these substrates in a similar manner, which strongly suggests that the control of cellular responses involves events downstream of the initial recognition step. These structures also allow us to map known cancer-causing mutations onto the structure of MutSα, a critical step in understanding the role of MutSα defects in cancer. Finally, these structures suggest plausible pathways for interdomain communication in MutSα.

## RESULTS

### The Structure of MutSα

We have solved the structure of full-length MSH2 opposite a protease-resistant fragment of MSH6 lacking the first 340 amino acids (MSH6Δ341), in complex with a series of DNA substrates (Figure 1). This heterodimer retains near wild-type activity in in vitro mismatch repair assays (Figure S1 and Supplemental Experimental Procedures in the Supplemental Data available with this article online). The MutSα heterodimer forms an asymmetric oval disc ~125 Å tall, 110 Å wide, and 65 Å thick, pierced by two channels like the letter "θ" (Figure 1A), with the MSH2 and MSH6 subunits lining the sides along the long axis. The two ATPase domains, one contributed by each subunit, are located at one end of the oval. A DNA helix containing a single mispair is bent by ~45° and bound in the larger of the two channels, the farthest from the ATPase domains (Figure 1B). Only MSH6 makes specific contacts with the mispaired bases, consistent with mutagenesis data (Dufner et al., 2000). MSH6 and MSH2 are pseudosymmetric and share a common domain architecture with prokaryotic mismatch proteins, Figure 1D, but differ in length and sequence (Figure 2B). Each protein can be divided into five domains, which we refer to as the mismatch binding domain, connector, levers, clamps, and ATPase domains, by analogy with the previously described *E. coli* structure (Lamers et al., 2000). Although the domain architecture of human and prokaryotic proteins is similar, the structures differ in detail and in domain orientation. The MutSα heterodimer is quite asymmetric—MSH6 and MSH2 superimpose with a Cα root-mean-square deviation (rmsd) of 5.5 Å.

The mismatch binding domain (domain 1) contains amino acids 1–124 of MSH2 and 362–518 of MSH6. The domain is mixed α/β in structure (Figure 2, blue ribbon). The protein-DNA interface in MutSα-DNA complexes (Figure 5E) differs from that in prokaryotic structures, in which domain 1 of the nonmismatch binding monomer (equivalent to MSH2) makes extensive contacts with the DNA backbone (Lamers et al., 2000; Obmolova et al., 2000). By contrast, domain 1 of MSH2 is rotated up and away from the DNA backbone and makes only one contact with the DNA (Figures 1B and 5E), consistent with the recent observation that MSH2 domain 1 is dispensable for mismatch repair by yeast MutSα (Lee et al., 2007). The N-terminal 14 amino acids of MSH2 form an extended strand that blocks the DNA binding face of the domain (Figure 4C) and packs against domain 1 of MSH6. The mismatch binding domains in prokaryotic structures do not interact with one another (Lamers et al., 2000; Obmolova et al., 2000). The MSH6 construct used in this work contains an additional ordered region at the N terminus of MSH6 (residues 360–398) that forms an extended region of coil with a large number of positively charged residues (Figure 1B). A derivative deletion mutant lacking this region no longer binds cellulose derivatized with single-stranded DNA (data not shown), consistent with a role in nonspecific DNA binding. Such nonspecific interactions may stabilize MutSα complexes with substrates such as C•C mispairs, which are not recognized by prokaryotic MutS proteins but can be recognized by the human repair system (Iyer et al., 2006; Kunkel and Erie, 2005).

The connector domain (domain 2) consists of residues 125–297 of MSH2 and 519–717 in MSH6. The domain has a mixed α/β structure (Figure 2, green). The domain packs into a cleft formed by domains 5 and 3 and appears well positioned to be involved in allosteric signaling

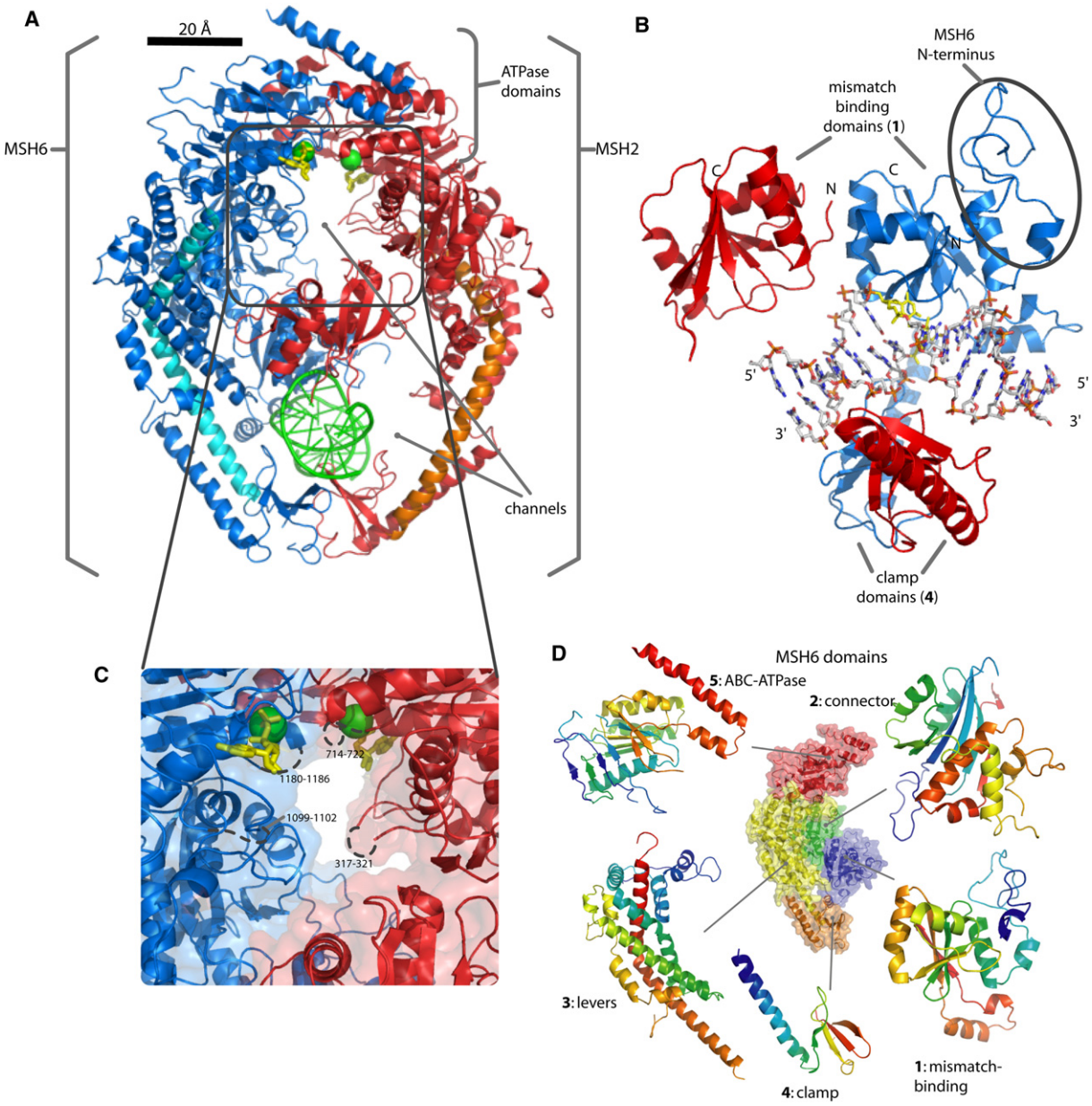


**Figure 1. Overview of the Structure of Human MutSα**

(A) Ribbon diagram of the structure of a MutSα/ADP/G•T mispair complex. Blue, MSH6; red, MSH2; green ribbon, DNA; yellow, ADP; and green spheres, $Mg^{2+}$ ions. Positions of the ABC ATPase domains and the two channels in MutSα are indicated. Long α helices connecting clamp and ATPase domains in MSH2 and MSH6 are colored orange and cyan, respectively.

(B) Orthogonal, expanded view of the DNA binding domains of MutSα. DNA is shown as sticks, colored by atom type, with the central G•T mispair colored yellow.

(C) Expanded view of the upper channel in MutSα, colored as in (A) and shown as ribbons and a transparent surface. Disordered loops are shown as dashed lines with residue numbers.

(D) The domain structure of MSH6. Center: domains 1–5 are colored blue, green, yellow, orange, and red, respectively. Periphery: exploded view of each domain, labeled and colored with blue-red "chainbows" from the N- to C termini of the domain. Figures were generated with PyMOL (DeLano, 2002).

between domains 3 and 5. The connection between domains 2 and 1 is through an extended strand, which may be flexible in the absence of DNA. The domains 1 and 2 in the two subunits of prokaryotic MutS homodimer structures have different relative orientations, which is also consistent with a flexible connection. Translation-libration-screw (TLS) refinement of thermal motions in X-ray crystal structures can be used to define independently moving

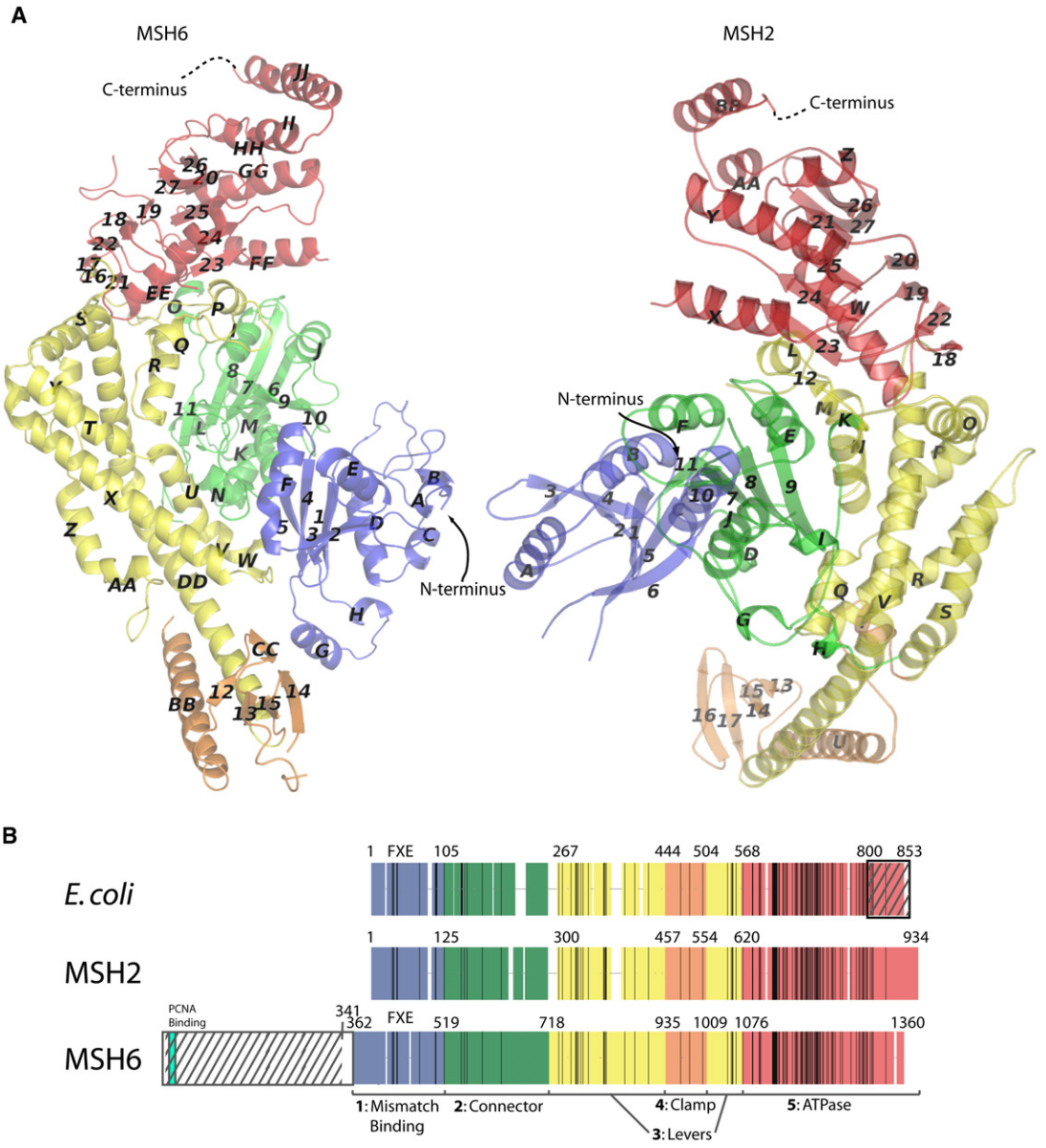


**Figure 2. Secondary and Primary Structure of MutSα**

(A) The secondary structure of MSH6 (left) and MSH2 (right) was defined with DSSP (Kabsch and Sander, 1983) and adjusted by visual inspection. Helices are assigned sequential letters, and β strands are numbered sequentially. Domains 1–5 are colored blue, green, yellow, orange, and red, respectively.

(B) Comparison of *E. coli* MutS, MSH2, and MSH6 primary sequences: domains colored as in (A); white space corresponds to gaps in the structure-based sequence alignment of the three proteins (see Figure S3); black lines indicate the location of residues that are identical in the three proteins; residue numbers indicate domain boundaries; and crosshatching indicates the portion of *E. coli* MutS removed for structural studies (Lamers et al., 2000) and the portion of MSH6 deleted in this study. The location of the conserved Phe-X-Glu motif in MutS and MSH6 is indicated with "FXE."

subdomains of macromolecules and the directions of movement (Chaudhry et al., 2004; Painter and Merritt, 2006; Wilson and Brunger, 2003). TLS refinement of MutSα reveals that domain 1 of MSH2 moves in an uncoupled manner from the remainder of the protein (Figure S2). Both MSH2 and MSH6's domain 2s have three surface loops, not conserved in prokaryotic MutS proteins, which may mediate protein-protein interactions. These comprise amino acids 150–160, 207–217, and 243–262 in MSH2 and 545–555, 602–612, and 650–675 in MSH6.

The long α-helical lever domain (domain 3) consists of residues 300–456 and 554–619 of MSH2 and 718–934 and 1009–1075 of MSH6 (Figure 2A, yellow). One striking feature of this domain in both human and prokaryotic

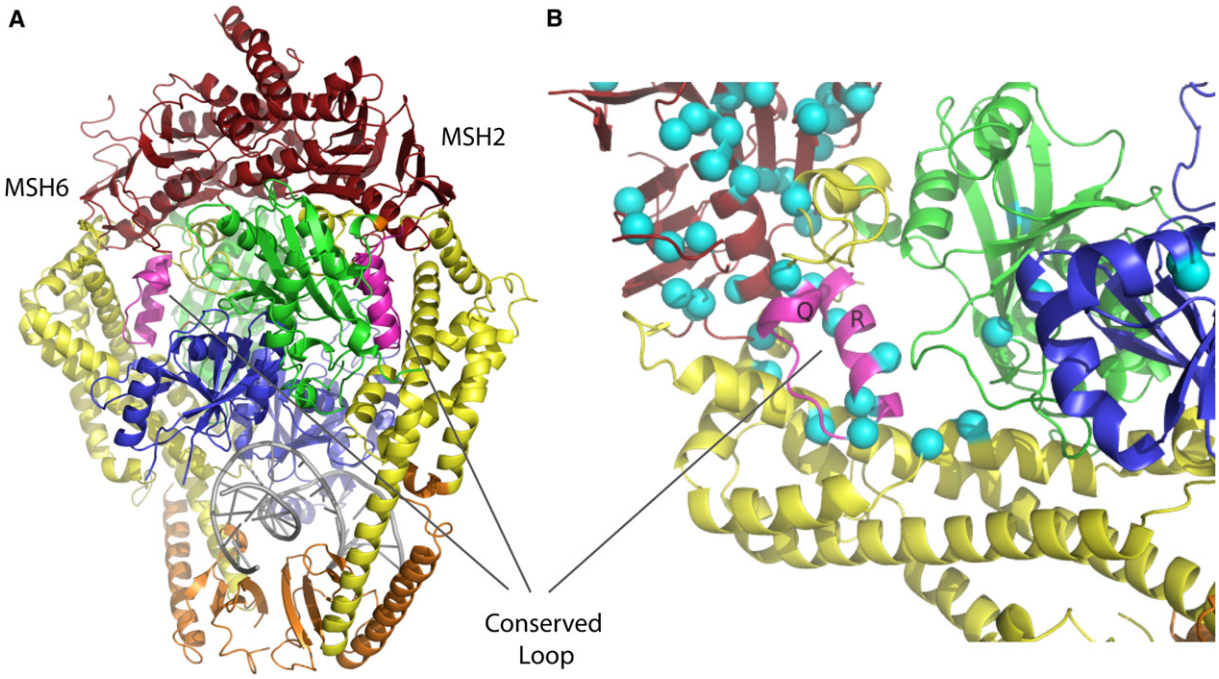


**Figure 3. A Conserved Loop at the Domain 2/3/5 Interface**

See Figure 2 for domain numbering.

(A) Location of the loops (magenta) in MSH6 (left) and MSH2 (right). MSH2 and MSH6 are colored by domain as in Figure 2.

(B) Close up of the loop in MSH6, colored as in (A). Cα positions of residues that are universally conserved among *Taq*, *E. coli*, and yeast and human MSH2 and MSH6 are shown with blue spheres. Note the concentration of conserved residues in domain 5 and in the vicinity of the loop. The two helices of the conserved loop are labeled as in Figure 2A.

structures is an ~60 amino acid long α helix (MSH2 helix V or MSH6 helix DD) in both MSH2 and MSH6 that spans the entire distance between domain 4 and domain 5 (Figures 1A and 2A). The sequence conservation in domain 3 is generally quite low. One exception to this trend is a conserved loop, amino acids 757–782 in MSH6, that lies at the intersection of domains 3, 2, and 5 and with helix V or DD in MSH2 or MSH6, respectively (Figure 3). Given the location and conservation of this region of the protein, this loop seems likely to be involved in signal transduction between the ATPase and DNA binding domains.

The clamp domains (domain 4) are small, largely β strand domains that are inserted between the two halves of domain 3 (Figure 2A, orange). They comprise amino acids 457–553 of MSH2 and 935–1008 of MSH6. Based on our TLS refinement results, we include a short α-helical segment (MSH2 helix U and MSH6 helix BB) in domain 4. These domains make significant nonspecific DNA contacts (Figure 5E). MSH6 domain 4 makes extensive contacts along a six base pair stretch of essentially B form DNA on one side of the mispair. MSH2 domain 4 makes contacts with bases on both sides of the mispair.

Domain 5, the ABC-ATPase domain, is the most highly conserved region of MutS homologs—domains 5 from *E. coli* and hMSH2 are 48% identical. Domain 5 consists of residues 620–855 in MSH2 and 1076–1355 in MSH6. These domains share the bilobed mixed α β structure typical of ABC transporters (Figure 2, red). Each adenosine-nucleotide binding site consists of residues from each protomer, and together the two ATPase domains form two composite ATPase sites (Figure 6, below). The C termini of both domain 5s form conserved helix-turn-helix motifs that interact with domain 5 of the opposed protomer. This interaction stabilizes the ABC-ATPase dimer interface even in the absence of ATP binding, which is required for dimerization of canonical ABC-transporter ATPase domains.

Both MSH2 (943 amino acids) and MSH6Δ341 (1020 aa) are larger than the C-terminally truncated variants of *E. coli* (800 aa) and *T. aquaticus* (768 aa), which were previously described (Lamers et al., 2000; Obmolova et al., 2000). Loss of the C terminus has been shown to severely compromise the function of *E. coli* MutS (Calmann et al., 2005). Although our crystallized MutSα complex has intact C termini for both MSH2 and MSH6, these regions are not well ordered in our electron density. We do see several regions of additional, likely helical electron density in solvent channels, which are consistent with all or part of the missing regions forming ordered domains connected to the body of MutSα by a flexible linker.

Both MSH2 and MSH6 have a number of loops that are disordered in our structure. Several cluster around the upper, empty channel through the heterodimer (Figure 1C). This opening is smaller than the analogous opening in

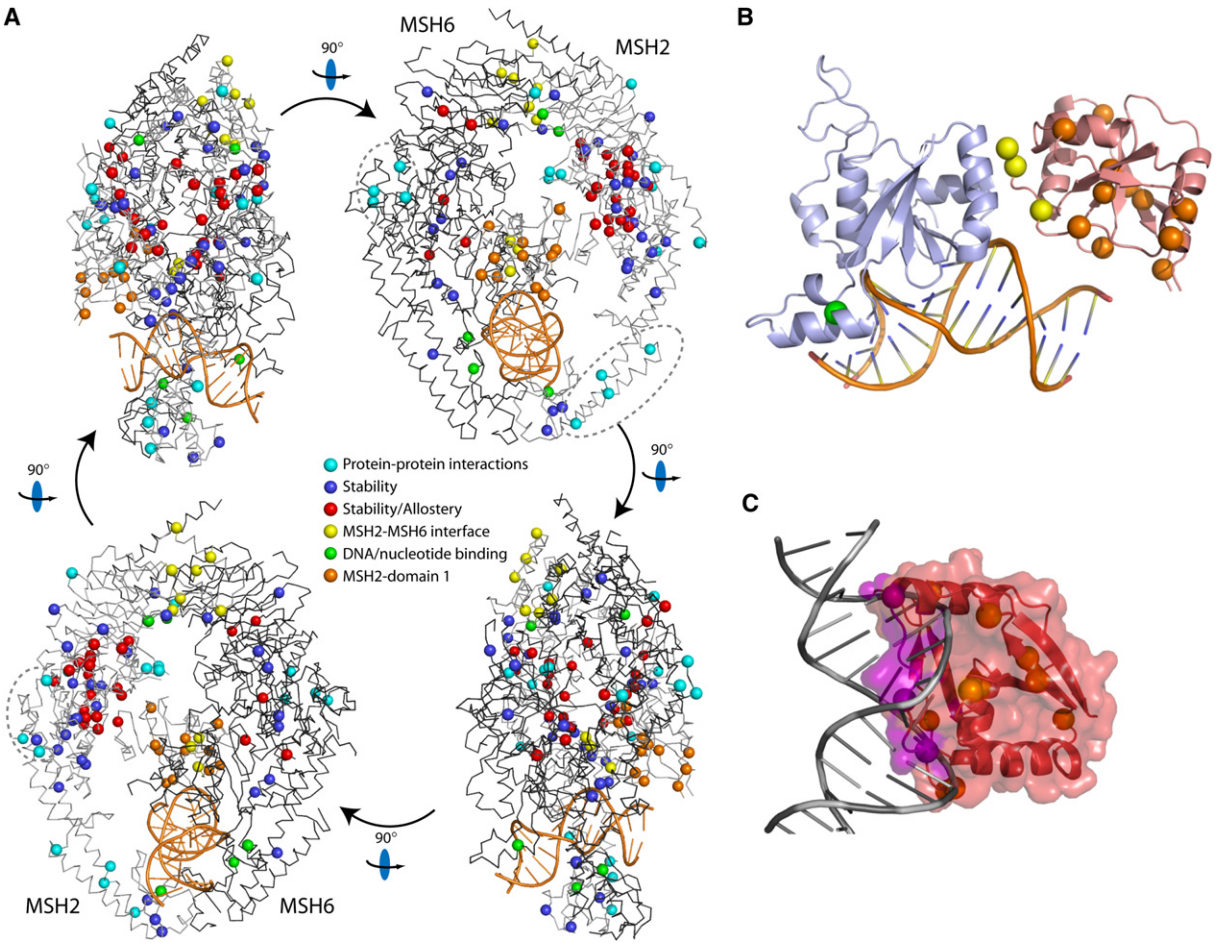


**Figure 4. HNPCC Mutations Mapped onto the Structure of MutSα**

(A) Four views of MutSα related by 90° rotations as indicated, with positions of HNPCC missense mutations indicated by spheres. Hypothetical functional classification of mutations is indicated by sphere color (see text and legend). MSH2 and MSH6 are shown as light and dark gray Cα chain traces, respectively, and the DNA is colored orange. Three clusters of surface mutations, which may correspond to sites of protein-protein interactions are indicated with dashed ovals.

(B) HNPCC mutations in domain 1 of MSH2 (red) and MSH6 (blue) shown as spheres, colored as in (A).

(C) An extended strand at the N terminus of MSH2 blocks its DNA binding face. DNA is shown as a gray ribbon and MSH2 as a red cartoon with a semi-transparent surface. Clashes that result from docking the DNA into the MSH2 binding site are shown in magenta.

prokaryotic structures—too small to accommodate a second DNA strand as has been previously proposed (Kunkel and Erie, 2005), even without taking the presence of these additional disordered regions into account. These disordered loops may be involved in communication between the ATPase and mismatch binding domains or may mediate protein-protein interactions.

## Structure-Based Sequence Alignments

We used the structure of MutSα to generate a structure-based sequence alignment of MSH2, MSH6, *T. aquaticus* MutS, and *E. coli* MutS, which we overlaid with a sequence alignment of *S. cerevisiae* MSH2 and MSH6 (Figure S3) to facilitate application of biochemical work in genetically tractable systems to human proteins and to enable choice of prokaryotic and yeast mutations that model mutations in human cancer. Mapping the sequence conservation of MSH2 and MSH6 onto the structure reveals that conserved amino acids are concentrated in the ATPase domains and generally on the inner surfaces of the two molecules, lining both the upper and lower (DNA binding) channels (Figure S4).

## MutSα and Hereditary Colon Cancer

To date, about 400 mutations in four MMR genes (*msh2*, *msh6*, *mlh1*, and *pms2*) have been reported to cause HNPCC, with about half of the mutations in the genes that code for MSH2 and MSH6, the components of MutSα (Peltomaki, 2003; Stenson et al., 2003; InSight database: http://www.insight-group.org/). HNPCC missense mutations are broadly distributed in all domains of both subunits (Figure 4A). Many of these mutations lie in regions of low

homology between prokaryotic and eukaryotic proteins, making location of analogous mutations in prokaryotes challenging. The structure of MutSα will allow structure-based comparisons of low-homology regions, which will facilitate the evaluation of the phenotypes of these mutations in genetically tractable organisms, leading to more accurate genetic counseling and more effective chemotherapy.

The effects of these mutations can be expected to fall into six broad classes: interference with DNA binding, loss of ATPase activity, loss of allosteric communication between DNA and ATP binding sites, loss of protein-protein interactions with downstream effectors, loss of MSH2-MSH6 interaction, and general loss of protein stability. A number of these mutations may be expected to have multiple effects; however, we have undertaken an initial hypothetical assignment of known HNPCC mutations to each of these classes (Figure 4A). We have identified three groups of mutations that lie in clusters on the surface of MutSα (circled in Figure 4A) that may define protein-protein interaction interfaces. Additionally, 14 unique HNPCC mutations are found in MSH2 domain 1 (Figure 4B). The observation of these mutations is challenging to rationalize with the fact that the domain has been shown to be dispensable for yeast MutSα function (Lee et al., 2007). This domain does not play a significant role in DNA binding (Figures 4B and 4C), and the distribution of mutations throughout the domain rather than on the surface points to a role other than protein-protein interactions. The fact that three HNPCC mutations map to the MSH2/MSH6 domain 1 interface may indicate that this intersubunit interaction is important for MutSα function (Figure 4B).

## DNA Substrate Recognition by MutSα

In MutSα-G•T complexes, domain 1 of MSH6 interacts extensively with the DNA mispair. Glu434 of the conserved Phe-X-Glu motif hydrogen bonds to the mispaired thymine, which is sandwiched between Phe432 and Met459, and the backbone carbonyl of Val429 accepts a hydrogen bond from the mispaired guanine (Figures 5A–5C). These interactions along with additional nonspecific protein-DNA interactions (Figure 5E) widen the DNA minor groove in the vicinity of the mispair, tilting the mispaired thymine so that its $O^4$ carbonyl interacts with the Watson-Crick face of the mispaired guanine. These interactions are similar to prokaryotic MutS interactions with DNA substrates (Lamers et al., 2000; Natrajan et al., 2003; Obmolova et al., 2000), indicating that the mechanism of DNA binding has been conserved in MutS homologs. Contacts with domain 1 of the nonmismatch binding monomer have been hypothesized to contribute to DNA bending in *Taq* MutS/DNA complexes (Obmolova et al., 2000); however, MSH2 does not make similar interactions. Interactions between MSH6 and the DNA substrate bury 1142 $Å^2$ of protein surface area (with domain 1 contributing 856 $Å^2$), which is probably sufficient to bend the DNA without any contribution from MSH2. Because MutSα binds substrates (such as C•C mispairs) that will be unable to make favorable nucleotide-nucleotide hydrogen bonds or to hydrogen bond with Glu434, it is likely that these nonspecific protein-DNA interactions are also sufficient for binding of deformable DNA substrates.

## A Common Binding Mode for MutSα DNA Complexes

We have solved a series of crystal structures of human MutSα bound to several DNA substrates that allow us to probe the nature of MutSα substrate recognition and which have important implications for the involvement of MutSα in cellular pathways other than repair (Table 1). These substrates include duplex DNAs containing a G•T mispair or a single base T insertion/deletion loop, which resemble DNA biosynthetic errors; an $O^6$-methyl-guanine•T mispair, which should resemble complexes that signal MMR-dependent cell death; or a G•dU mispair, a putative intermediate in somatic hypermutation (Wilson et al., 2005). Strikingly, both G•U (Figure 5B) and $O^6$-methyl-guanine•T complexes (Figure 5C) are virtually identical to the G•T mispair (Figure 5A), with Cα rmsds of 0.43 and 0.42 Å, respectively, to the original G•T structure. Although a T insert is expected to be repaired in a MutSα-dependent manner (Drummond et al., 1995), our T insert structure differs somewhat from that of the G•T mispair; accommodating the unpaired T without disrupting neighboring base pairs requires a change in the bend angle at the mispair, although the overall bend is not changed (Figures 5D and 5F). Slight motions of the helical arms of domain 3 and a movement of domain 4 of MSH2 allow this adjustment to occur without compromising the nonspecific interactions between domains 4 of MSH2 and MSH6 and the DNA backbone (Figure 5F).

The presence of the negatively charged glutamate in the MSH6 Phe432-Glu434-Met459 binding pocket (Figure 5A) will likely cause some lesions, such as T•C mispairs or T inserts, to show a preference for one orientation of the MutSα heterodimer (in these examples with MSH6 bound to the thymine). This asymmetry of the heterodimer may have implications for the downstream activities of MutSα, which must be capable of initiating repair in the correct direction from a nick either 3′ or 5′ to the mispair.

## ATPase Sites

We have solved structures of MutSα in two nucleotide-bound states, with one or two molecules of ADP bound in the ATPase sites of the heterodimer, respectively. Genetic and biochemical characterization of mutations in the conserved ABC-ATPase domains of MutS homologs has demonstrated the central role played by these domains in the MutSα reaction cycle (Iyer et al., 2006; Kunkel and Erie, 2005). ABC-transporter ATPases function as homo- or heterodimers with two composite ATPase sites, each consisting of a Walker A and Walker B motif from one monomer and the ABC signature motif from the alternate monomer. Isolated ABC-transporter ATPase domains require ATP binding to form stable dimer interfaces and disengage in the presence of ADP (Locher, 2004), and

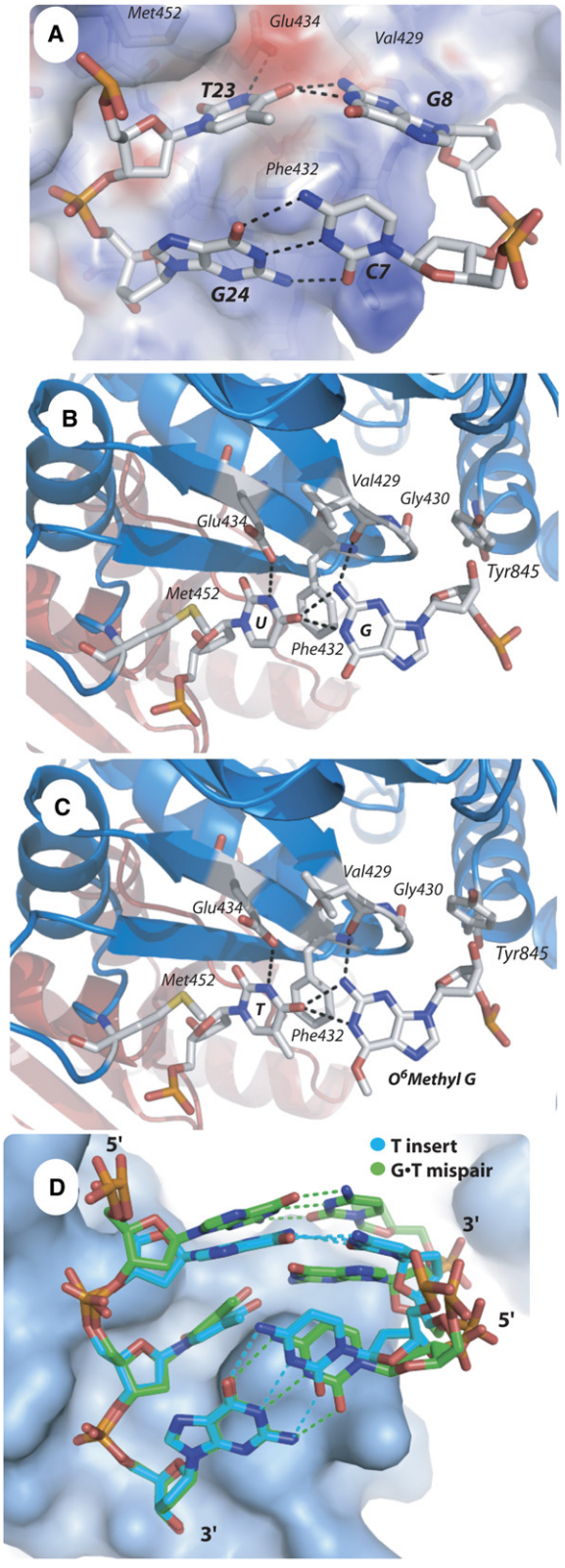
A
Met452
Glu434
Val429
T23
G8
Phe432
C7
G24
B
Val429
Gly430
Glu434
Tyr845
Met452
U
G
Phe432
C
Val429
Gly430
Glu434
Tyr845
Met452
T
Phe432
O6Methyl G
D
5'
T insert
G•T mispair
3'
5'
3'
E
5'
3'
G1
C30
A2
T29
A3
T28
C4
G27
C5
G26
G6
C25
C7
G24
C9
G22
G10
C21
C11
G20
T12
A19
Lys 1000
Thr 999
Lys 1004
Trp 970
Ile 972
MSH2
domain 4
MSH6
domain 4
Gln 518
MSH2
domain 1
Gln 545
Ile 464
Ala 465
Lys 6
Lys 546
Pro 462
Arg 468
Asn 975
Phe 461
Tyr 469
Leu 449
Phe 432
Gly 460
Arg 974
Lys 431
Val 450
G8
T23
MSH6
domain 1
Gly 430
Glu 434
Met 452
Val 429
Lys 453
Val 509
Arg 511
Val 508
MSH2
domain 4
Met 410
Pro 408
Gly 409
Lys 512
Arg 524
Thr 407
F
domain 1
domain 3
T insert
G•T
domain 4

**Table 1. Crystallographic Data and Refinement Statistics**

| Structure | G•T | G•dU | O6MeG•T | T Insert | MSH6 Nucleotide Free |
|---|---|---|---|---|---|
| PDB code | 2O8B | 2O8D | 2O8C | 2O8F | 2O8E |
| Space group | $P4_332$ | | | | |
| Unit cell a (Å) | 258.74 | 260.35 | 259.81 | 259.55 | 259.10 |
| Beamline | NSLS X25 | APS 22ID | APS 22ID | APS 22ID | APS 22ID |
| λ (Å) | 1.0065 | 0.97931 | 1.0 | 1.0 | 1.0048 |
| Resolution range (Å)[a] | 50–2.75(2.82–2.75) | 50–3.0(3.25–3) | 50–3.37(3.556–3.37) | 50–3.25(3.33–3.25) | 50–3.3(3.4–3.3) |
| Total reflections | 719,762 | 362,531 | 408,727 | 311,481 | 770,486 |
| Unique reflections | 76,366 | 60,518 | 42,279 | 47,220 | 45,130 |
| Completeness[a] | 99.8 (97.9) | 99.8 (100) | 99.2 (98.6) | 99.7 (99.8) | 99.9 (100) |
| Multiplicity[a] | 9.4 (5.8) | 6.0 (6.2) | 9.7 (7.9) | 6.6 (5.9) | 17.1 (17.4) |
| I/σ(I)[a] | 19.7 (2.6) | 14.2 (3.2) | 14.2 (3.3) | 9.9 (2.4) | 21.0 (3.4) |
| $R_{sym}$[a] | 0.094 (0.504) | 0.093 (0.584) | 0.148 (0.517) | 0.129 (0.492) | 0.131 (1.065) |
| Final Model | | | | | |
| Refinement resolution[a] | 20-2.75(2.82-2.75) | 50-3(3.078-3) | 20-3.37(3.455-3.37) | 20-3.25(3.33-3.25) | 50-3.33.386-3.3 |
| Number of nonhydrogen atoms | 14,641 | 14,640 | 14,624 | 14,739 | 14579 |
| Number of waters | 46 | 46 | 28 | 46 | 14 |
| $R_{work}$[a] | 0.246 (0.344) | 0.239 (0.317) | 0.256 (0.312) | 0.246 (0.41) | 0.243 (0.301) |
| $R_{free}$[a] | 0.285 (0.390) | 0.278 (0.332) | 0.290 (0.325) | 0.296 (0.44) | 0.286 (0.332) |
| Rmsd bonds (Å) | 0.014 | 0.007 | 0.006 | 0.01 | 0.008 |
| Rmsd angles (°) | 1.54 | 1.342 | 1.13 | 1.72 | 1.362 |
| Ramachandran favored (%) | 91.62 | 91.68 | 92.08 | 90.59 | 90.81 |
| Ramachandran allowed (%) | 99.48 | 99.42 | 99.42 | 99.31 | 99.08 |
| Bad rotamers (%) | 0.39 | 0.19 | 0 | 0.13 | 0.52 |
| Clash score | 12.53 | 9.97 | 8.76 | 6.85 | 11.75 |

[a] Values in parentheses refer to the highest resolution bin.

a cycle of engaging, ATP hydrolysis, and ADP dissociation is thought to drive the transport of substrates through ABC transporters. By contrast, in MutSα•DNA complexes, helix-turn-helix motifs at the C termini hold the ATPase domains in an orientation that resembles the engaged, ATP-bound complex seen in ABC-transporter structures even in the absence of ATP (Figure 6A).

It has previously been shown that the two ATPase sites in MutSα have different nucleotide affinities (Antony and Hingorani, 2003; Martik et al., 2004), and crosslinking

**Figure 5. Common Binding Mode for MutSα Substrates**

(A) Interactions between a G•T mispair and an adjacent base pair with MSH6 domain 1 (shown as sticks under a semitransparent electrostatic surface).

(B) Protein-mispair contacts in a MutSα/G•dU/DNA complex. Putative hydrogen bonds are shown as dashed lines. Interacting residues (defined with LIGPLOT [Wallace et al., 1995]) are labeled. Orientation is rotated ~90° from (A).

(C) Protein mispair contacts in a MutSα/$O^6$-methyl-guanine/DNA complex, colored, labeled, and oriented as in (B).

(D) Interactions between a single base T insert substrate (cyan carbons) or a G•T mispair (green carbons) substrate and MSH6 domain 1 (blue surface). Hydrogen bonds are shown as dashed lines. Orientation is approximately the same as (A).

(E) Protein-DNA interactions in the MutSα-DNA complex. Amino acids that make hydrogen bonding (red lines) or van der Waals interactions (gray lines) are indicated with blue text (MSH6) or red text (MSH2). Dashed lines group the amino acids by protein domain as indicated. Interactions were classified by using Probe (Word et al., 1999).

(F) Structures with G•T (red), T insert (green) were superimposed on domain 1 of MSH6. DNAs from both complexes are shown as sticks, and backbone traces of MSH2 are shown as ribbons and surfaces. The arrow indicates the movement of domains 4 and 3 of MSH2 in the insert structure that compensates for the slight change in the DNA substrate register.

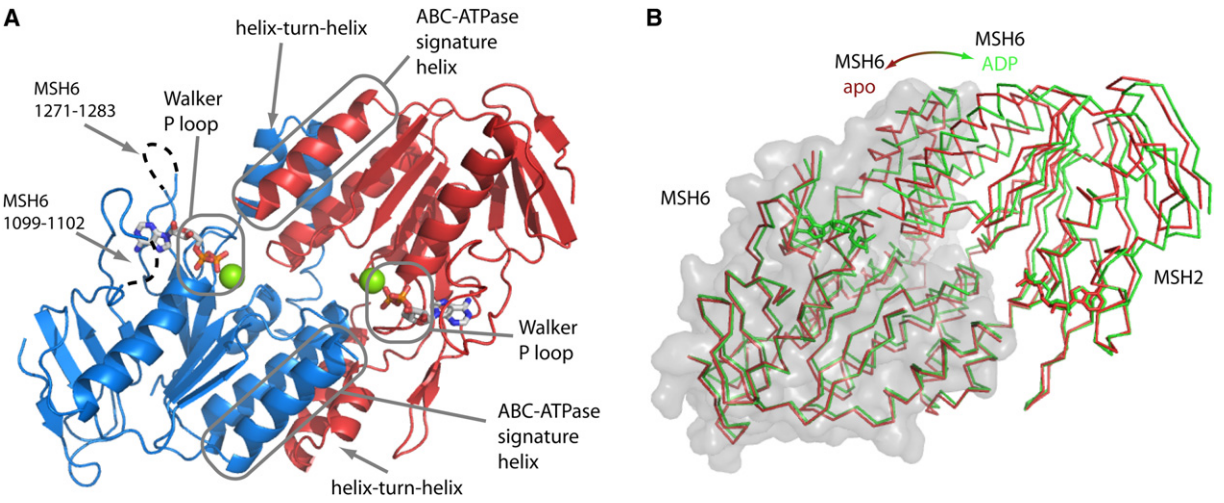


**Figure 6. Composite ABC-ATPases of MutSα**

(A) MutSα with ADP and $Mg^{2+}$ (green spheres) bound to the active sites of MSH6 (blue) and MSH2 (red). Conserved features of ABC transporters and the helix-turn-helix motif conserved in MutS proteins are indicated. The ABC-transporter signature motifs are found at the MSH6/MSH2 interface at the N termini of the α helices marked "ABC signature helix." Dashed lines indicate disordered loops in MSH6.

(B) Movements of MSH2 domain 5 and the MSH6 helix-turn-helix motif in the absence of bound nucleotide by MSH6. MSH6-apo and ADP-bound structures (superimposed on MSH6, domain 5) are shown as red and green Cα chain traces, respectively. MSH6 is enclosed in a transparent gray surface to distinguish it from MSH2.

experiments in yeast (Mazur et al., 2006) and humans (Lored Asllani and P.L.M., unpublished data) have identified MSH2 as the high-affinity ADP site. This is consistent with our observation that in the absence of added nucleotide we still observe a single MSH2-bound ADP that copurifies with MutSα. Crystallization of MutSα/DNA complexes in the presence of ADP or ATP (which can be hydrolyzed by the ATPase domains) yields complexes with ADP bound to both MSH2 and MSH6 (Figure 6A). The ATPase sites of MSH2 and MSH6 with bound ADP are virtually superimposable. However, the MSH2 ATPase site is bracketed by two well-ordered loops, whereas the corresponding loops in MSH6 are partially disordered (Figure 6A). Thus, the differences in ADP binding affinity of the two domains are likely a result of increased dynamics of MSH6 domain 5. When no ADP or ATP is added during crystallization, the phosphate binding loop of the Walker A motif (Walker et al., 1982) in the apo-MSH6 ATPase site collapses and domain 5 shifts toward MSH2 by about half an α-helical turn (Figure 6B). The observation of tighter ADP binding by MSH2 differs from the observation in prokaryotic MutS that the mismatch binding monomer has higher ADP affinity (Lamers et al., 2000).

In the absence of DNA at equilibrium, MutSα primarily exists in a state with one ADP and one ATP bound (Antony and Hingorani, 2003; Martik et al., 2004). The observation that ATP binding to *E. coli* MutS reduces affinity for DNA heteroduplexes (Blackwell et al., 2001) implies that the converse must also be true and heteroduplex binding must reduce ATP affinity. This explains the state observed in our structures, in which the protein makes specific contacts with the mispair, allosteric activation of ATP hydrolysis has presumably occurred, and both MSH2 and MSH6 are bound to ADP. Binding to DNA in this conformation likely requires both DNA bending and the binding of one nucleotide to the pocket produced by Phe432, Glu434, and Met454.

## DISCUSSION

### The Diverse Roles of MutSα in Cellular Responses to DNA Lesions

The observation that mutations in MutSα can confer resistance to DNA methylating agents led to the proposal that MutSα may act as a sensor of genetic damage in a repair-independent manner (Kat et al., 1993). The identification of mutations in MutSα that eliminate repair functions without reducing the MutSα-dependent damage response appears to support this model (Drotschmann et al., 2004; Lin et al., 2004). On the other hand, $O^6$-methyl-guanine•T pairs are isosteric to G•C pairs in DNA polymerase active sites, which causes frequent misinsertion of T opposite $O^6$-methyl-guanine (Warren et al., 2006), and the observation that human cells treated with methylators arrest in the second G2 after treatment suggests that damage signaling requires mutagenic translesion synthesis, followed by lesion processing by the MMR system (Goldmacher et al., 1986). Hsieh and coworkers recently suggested that the requirement for translesion synthesis results from a specificity of MutSα for $O^6$-methyl-guanine•T mispairs and that in the presence of these lesions MMR proteins can directly recruit checkpoint signaling factors to the site of damage in the absence of repair (Yoshioka et al., 2006). This finding is controversial, because MutSα binding of $O^6$-methyl-guanine•C mispairs had previously been reported (Duckett et al., 1996; Rasmussen and

Samson, 1996). Further, Jiricny and coworkers reported colocalization of the checkpoint signaling protein ATR and the single-strand binding protein RPA at damage foci, indicating that excision has occurred at damage sites (Stojic et al., 2004).

If MutSα indeed serves as a gatekeeper, shuttling different substrates into appropriate pathways for repair or other cellular responses, then binding to different classes of lesions must give rise to structural changes that alter the interactions with downstream effectors. However, we observe that the MutSα complex with $O^6$-methyl-guanine•T is not different from that with a G•T mispair. Similarly, a MutSα/G•U mispair complex resembles ones subject to the canonical mismatch-repair reaction, in spite of the fact that these substrates may be processed differently in diversifying B cells (Rada et al., 1998; Wilson et al., 2005). The similar mode of recognition utilized by MutSα in its interaction with different DNAs contrasts strikingly with the profound structural heterogeneity in DNA polymerase complexes with mispairs (Johnson and Beese, 2004) and is surprising given the significant differences in DNA base pairing, conformation, and thermal stability that these sequences would be expected to exhibit when free in solution. Although we cannot eliminate the possibility that MutSα may bind damaged DNA substrates differently under other conditions, our observation of a single mode of MutSα-DNA binding in complexes with substrates that elicit distinct cellular responses indicates that MutSα itself is unlikely to modulate cellular responses to these different substrates. Presumably, therefore, other downstream effectors are responsible for directing outcomes.

These observations might appear incongruent with reports of mutations in the ATPase domains of yeast and mouse MutSα that eliminate repair without compromising its cell-death functions. However, those uncoupling mutations that have been further characterized (such as the Walker A mutation equivalent to hMSH2 G764A) eliminate ATP-induced dissociation from mismatches and act as dominant-negative inhibitors of MMR (Alani et al., 1997; Drotschmann et al., 2004; Kijas et al., 2003; Lin et al., 2004; Studamire et al., 1998). These MutSα mutants may therefore bind to DNA lesions more stably than the wild-type protein, increasing the residence time of MutSα at these positions. A similar increase in residence time would be expected for MutSα engaged in futile cycles of failed repair with irreparable substrates, such as those with $O^6$-methyl-guanine lesions on the parental DNA strand (York and Modrich, 2006). If downstream effectors involved in the DNA damage response are triggered by the increased residence time of MutSα at lesions, then the divergent models for MutSα function can be reconciled.

## DNA Substrate Recognition

Like other DNA repair enzymes, MutSα must locate a subtle base pair anomaly within a vast excess of nonsubstrate, correctly paired DNA. Atomic force microscopy studies on prokaryotic MutS bound to DNA with and without lesions led to the proposal that correctly paired DNA binds in smoothly bent conformation, whereas mispairs make additional interactions with the protein, resulting in a more sharply localized kinked DNA conformation (Wang et al., 2003). An analogous mechanism is employed by base excision repair glycosylases (Banerjee et al., 2005, 2006), which bend all DNAs but only extrude substrate nucleotides into the enzyme active sites. A similar sequence of events may occur with MutSα-DNA complexes, with correctly paired MutSα-DNA complexes differing in conformation from lesion complexes. Alternatively, the difference between homoduplex and heteroduplex binding to MutSα may be kinetic, and the association with correctly paired DNA may be too transient for activation to occur.

## The Reaction Cycle of MutSα

Strand-specific excision of a DNA lesion by the MMR system requires signaling between the lesion and a nick or gap in a manner that retains information about the relative orientation of the two DNA sites. Three models have been put forward to explain this communication: MutSα induces DNA bending to bring mispair and nick into physical proximity (Schofield et al., 2001), MutSα moves along the helix contour from mispair to nick in an ATP-dependent manner (Modrich, 1987), or MutSα binding to a mismatch nucleates the polymerization of a second factor along the helix contour to the nick (Modrich, 1987). A minimal mechanism for MutSα in MMR must involve at least three states: a scanning state in which the heterodimer searches for a mispair or lesion, a mispair-bound state in which the protein complex associates specifically with its DNA substrate, and an activated state in which MutSα transmits information to a nick that confers strand specificity on the reaction. In each state, MSH2 and MSH6 may have a different set of nucleotide affinities and differing rates of ATP hydrolysis. This cycle is more complex than that of typical ABC transporters, which operate via a two-state mechanism in which the transporter channel is alternatively open to one side of the membrane or the other (Dawson and Locher, 2006). Achieving a mechanistic understanding of MutSα function requires determining both the manner in which substrate DNA binding drives allosteric activation of the ATP hydrolytic centers and the way in which conformational changes in the ATPase domains activate downstream repair events. Although definitive structural answers to these questions must await solution of complexes with homoduplex DNA and in additional nucleotide states, our structures and previous work in the field suggest several hypotheses.

The interfaces that connect relatively rigid domains may be critical sites for allosteric communication in proteins (Schirmer and Evans, 1990). Analysis of TLS refinement of thermal motions can provide information about the boundaries of such domains (Chaudhry et al., 2004; Painter and Merritt, 2006; Wilson and Brunger, 2003). Examination of our structure suggests critical regions of the

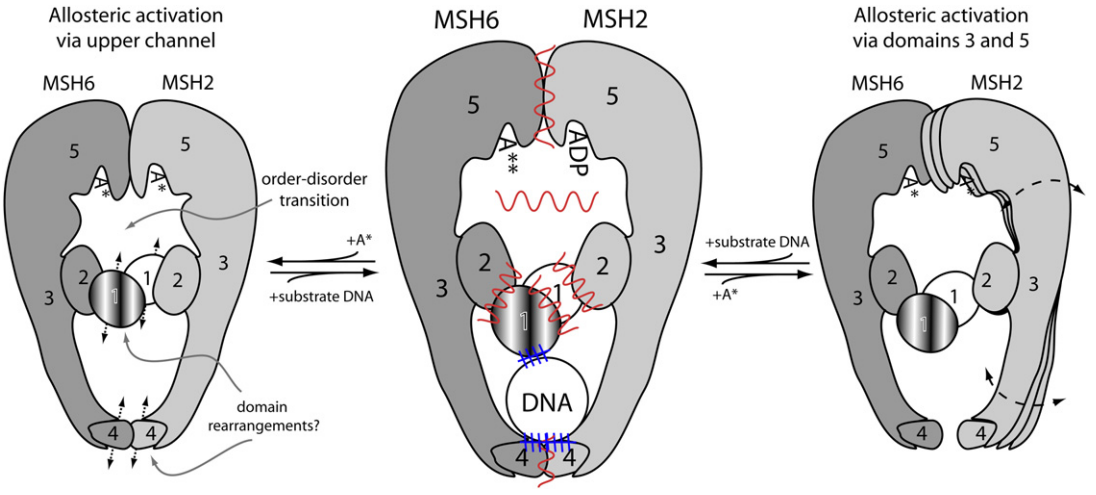


**Figure 7. Allosteric Communication between the DNA Binding and ATPase Sites of MutSα**

Mobile structural elements, locations of interdomain interfaces, and regions that may undergo order-disorder transitions are indicated schematically. (Center) Schematized view of the MutSα heterodimer. Domains are numbered, and regions that likely move independently are shaded differently. Blue hatching indicates positions of protein-DNA interactions. Red lines indicate positions of likely conformationally responsive interdomain interfaces (although we cannot exclude the possibility that other domain boundaries may serve such a role as well). We have observed MutSα•DNA complexes with either ADP or no nucleotide in the ATPase site (indicated as A**) of MSH6 (see text). (Left) An order-disorder equilibrium in loops in the upper channel, perhaps with accompanying domain rearrangements of domains 1 and 2 may disrupt DNA binding either leading to DNA dissociation (as shown) or to adoption of alternate DNA binding (such as an activated sliding mode). (Right) The rigidity of domains 5 and 3 may facilitate their involvement in coupling shifts in conformational equilibria in the ATPase domains to shifts in DNA binding equilibria in domains 1 and 4. Again, this may either lead to disruption of DNA binding (as shown) or the adoption of an alternate DNA binding mode. We cannot define the binding state of the ATPase sites (ADP, ATP, or empty) in the left and right panels (indicated as A*).

MutSα heterodimer that may serve as conformationally responsive interdomain interfaces (Figure 7). First, analysis of TLS refinement of thermal motions in MutSα (Figure S2) suggests that in both MSH2 and MSH6 domains 3 and 5 move together as a unit. Together these two domains span the length of the molecule and may serve to couple a DNA binding-induced conformational shift in domain 4 to alterations in nucleotide binding properties at the ATPase sites, ~100 Å away (Figure 7, right panel).

Second, the surface of the upper channel of the heterodimer is relatively highly conserved (Figure S4) and several HNPCC mutations are found here (Figure 4), indicating the importance of this region for function. A number of disordered loops border this channel (Figure 1C), including loops containing essential residues for ATP hydrolysis. Nucleotide binding and/or hydrolysis may modulate a disorder-order transition in this region (Dyson and Wright, 2002), which may also alter the conformations of domains 1 and 2 of MSH2 or MSH6. Conversely, DNA substrate binding may stabilize domains 1 and 2 in the conformations observed in our structures, effecting an order-disorder transition in the loops bordering the channel and altering nucleotide binding (Figure 7, left panel).

## MutSα Mutations and Human Disease

Mapping of HNPCC mutations suggests regions of the protein involved in its function and in interactions with downstream effectors. The observation that these mutations are broadly distributed throughout both protomers is consistent with the notion that allosteric coupling between ATPase and DNA binding sites plays a central role in the MutSα mechanism. In addition to providing a rigorous framework for biochemical dissection of the MutSα mechanism, the structure of MutSα will allow mapping of observed human mutations onto homologous proteins in genetically tractable organisms to rapidly evaluate the effects of these mutations. This may be particularly important for MutSα mutations that arise in sporadic cancers. These alleles may only slightly elevate mutation rates or confer only weak resistance to chemotherapeutic agents but may nevertheless confer an evolutionary advantage on the precancerous cells that harbor them. The ability to rapidly evaluate the effects of these mutations in *E. coli* or yeast should allow choice of more effective chemotherapies and allow more accurate genetic counseling of patients.

## EXPERIMENTAL PROCEDURES

### Construct

Full-length MSH2 was cloned into a baculovirus vector and expressed in *Sf9* cells opposite a protease-resistant fragment of MSH6 lacking the first 340 amino acids. This truncation is >90% active in 3′ directed and about 60% active in 5′ directed mismatch repair as scored by in vitro assay (Figure S1 and Supplemental Experimental Procedures).

### Structure Solution

MutSα DNA cocrystals were grown by vapor diffusion using PEG 8000 as a primary precipitant. The complex crystallizes in space group $P4_332$, with unit cell dimensions a = b = c = 260 Å, $\alpha = \beta = \gamma = 90^{\circ}$, and 24 molecules in the unit cell. Initial ~5 Å phases were obtained from a single-site $Ta_6Br_{12}$ derivative by single isomorphous replacement with anomalous scattering. These phases were used to locate selenium sites in selenomethionine-substituted MutSα crystals for MAD phasing (see Table 1). The final structure of MutSα/G•T/ADP had crystallographic R and $R_{free}$ values of 24/28 at 2.75 Å resolution. Additional structures were solved by Fourier synthesis from this starting model (see Table 1 and Supplemental Experimental Procedures). Representative omit density for DNA mispairs and representative experimental density are shown in Figure S5.

### Supplemental Data

Supplemental Data include Supplemental Experimental Procedures, Supplemental References, five figures, and one table and can be found with this article online at http://www.molecule.org/cgi/content/full/26/4/579/DC1/.

## ACKNOWLEDGMENTS

The authors thank James Phillips for assistance with data analysis, Lou Messerle and Daniel Hay for providing $Ta_6Br_{12}$, and Homme Hellinga for critically reading the manuscript. Data were measured at SER-CAT at the Advanced Photon Source, Argonne National Laboratory, financially supported by the U.S. Department of Energy (DOE), and at beamline X25 of the National Synchrotron Light Source, financially supported by the DOE and the National Institutes of Health. This work was supported by the Structural Cell Biology of DNA Repair Program Grant (5 PO1 CA92584) from the National Cancer Institute to L.S.B. and P.L.M., by grant GM45190 to P.L.M., by an Ellison Medical Foundation Fellowship of the Life Sciences Research Foundation to A.C., and by an Agouron Institute Fellowship from the Jane Coffin Childs Memorial Fund for Medical Research to J.J.W. P.L.M. is an Investigator of the Howard Hughes Medical Institute.

Received: November 29, 2006
Revised: March 22, 2007
Accepted: April 20, 2007
Published: May 24, 2007

## REFERENCES

Alani, E., Sokolsky, T., Studamire, B., Miret, J.J., and Lahue, R.S. (1997). Genetic and biochemical analysis of Msh2p-Msh6p: role of ATP hydrolysis and Msh2p-Msh6p subunit interactions in mismatch base pair recognition. Mol. Cell. Biol. *17*, 2436–2447.

Antony, E., and Hingorani, M.M. (2003). Mismatch recognition-coupled stabilization of Msh2-Msh6 in an ATP-bound state at the initiation of DNA repair. Biochemistry *42*, 7682–7693.

Banerjee, A., Yang, W., Karplus, M., and Verdine, G.L. (2005). Structure of a repair enzyme interrogating undamaged DNA elucidates recognition of damaged DNA. Nature *434*, 612–618.

Banerjee, A., Santos, W.L., and Verdine, G.L. (2006). Structure of a DNA glycosylase searching for lesions. Science *311*, 1153–1157.

Blackwell, L.J., Bjornson, K.P., Allen, D.J., and Modrich, P. (2001). Distinct MutS DNA-binding modes that are differentially modulated by ATP binding and hydrolysis. J. Biol. Chem. *276*, 34339–34347.

Calmann, M.A., Nowosielska, A., and Marinus, M.G. (2005). The MutS C terminus is essential for mismatch repair activity in vivo. J. Bacteriol. *187*, 6577–6579.

Chaudhry, C., Horwich, A.L., Brunger, A.T., and Adams, P.D. (2004). Exploring the structural dynamics of the E.coli chaperonin GroEL using translation-libration-screw crystallographic refinement of intermediate states. J. Mol. Biol. *342*, 229–245.

Dawson, R.J., and Locher, K.P. (2006). Structure of a bacterial multidrug ABC transporter. Nature *443*, 180–185.

DeLano, W.L. (2002). The PyMOL User's Manual (San Carlos, CA: DeLano Scientific).

Drotschmann, K., Topping, R.P., Clodfelter, J.E., and Salsbury, F.R. (2004). Mutations in the nucleotide-binding domain of MutS homologs uncouple cell death from cell survival. DNA Repair (Amst.) *3*, 729–742.

Drummond, J.T., Li, G.-M., Longley, M.J., and Modrich, P. (1995). Isolation of an hMSH2•p160 heterodimer that restores mismatch repair to tumor cells. Science *268*, 1909–1912.

Duckett, D.R., Drummond, J.T., Murchie, A.I.H., Reardon, J.T., Sancar, A., Lilley, D.M.J., and Modrich, P. (1996). Human MutSα recognizes damaged DNA base pairs containing $O^6$-methylguanine, $O^4$-methylthymine or the cisplatin-d(GpG) adduct. Proc. Natl. Acad. Sci. USA *93*, 6443–6447.

Dufner, P., Marra, G., Raschle, M., and Jiricny, J. (2000). Mismatch recognition and DNA-dependent stimulation of the ATPase activity of hMutSα are abolished by a F432A mutation in the hMSH6 subunit. J. Biol. Chem. *275*, 36550–36555.

Dyson, H.J., and Wright, P.E. (2002). Coupling of folding and binding for unstructured proteins. Curr. Opin. Struct. Biol. *12*, 54–60.

Goldmacher, V.S., Cuzick, R.A., and Thilly, W.G. (1986). Isolation and partial characterization of human cell mutants differing in sensitivity to killing and mutation by methylnitrosourea and *N*-methyl-*N'*-nitro-nitrosoguanidine. J. Biol. Chem. *261*, 12462–12471.

Iyer, R.R., Pluciennik, A., Burdett, V., and Modrich, P.L. (2006). DNA mismatch repair: functions and mechanisms. Chem. Rev. *106*, 302–323.

Jiricny, J. (2006). The multifaceted mismatch-repair system. Nat. Rev. Mol. Cell Biol. *7*, 335–346.

Johnson, S.J., and Beese, L.S. (2004). Structures of mismatch replication errors observed in a DNA polymerase. Cell *116*, 803–816.

Kabsch, W., and Sander, C. (1983). Dictionary of protein secondary structure: pattern recognition of hydrogen-bonded and geometrical features. Biopolymers *22*, 2577–2637.

Kat, A., Thilly, W.G., Fang, W.H., Longley, M.J., Li, G.M., and Modrich, P. (1993). An alkylation-tolerant, mutator human cell line is deficient in strand-specific mismatch repair. Proc. Natl. Acad. Sci. USA *90*, 6424–6428.

Kijas, A.W., Studamire, B., and Alani, E. (2003). Msh2 separation of function mutations confer defects in the initiation steps of mismatch repair. J. Mol. Biol. *331*, 123–138.

Kolodner, R.D. (1995). Mismatch repair: mechanisms and relationship to cancer susceptibility. Trends Biochem. Sci. *20*, 397–401.

Kunkel, T.A., and Erie, D.A. (2005). DNA mismatch repair. Annu. Rev. Biochem. *74*, 681–710.

Lamers, M.H., Perrakis, A., Enzlin, J.H., Winterwerp, H.H., de Wind, N., and Sixma, T.K. (2000). The crystal structure of DNA mismatch repair protein MutS binding to a G x T mismatch. Nature *407*, 711–717.

Lee, S.D., Surtees, J.A., and Alani, E. (2007). Saccharomyces cerevisiae MSH2-MSH3 and MSH2-MSH6 complexes display distinct requirements for DNA binding domain I in mismatch recognition. J. Mol. Biol. *366*, 53–66.

Lin, D.P., Wang, Y., Scherer, S.J., Clark, A.B., Yang, K., Avdievich, E., Jin, B., Werling, U., Parris, T., Kurihara, N., et al. (2004). An Msh2 point mutation uncouples DNA mismatch repair and apoptosis. Cancer Res. *64*, 517–522.

Locher, K.P. (2004). Structure and mechanism of ABC transporters. Curr. Opin. Struct. Biol. *14*, 426–431.

Martik, D., Baitinger, C., and Modrich, P. (2004). Differential specificities and simultaneous occupancy of human MutSalpha nucleotide binding sites. J. Biol. Chem. *279*, 28402–28410.

Mazur, D.J., Mendillo, M.L., and Kolodner, R.D. (2006). Inhibition of Msh6 ATPase activity by mispaired DNA induces a Msh2(ATP)-Msh6(ATP) state capable of hydrolysis-independent movement along DNA. Mol. Cell *22*, 39–49.

Modrich, P. (1987). DNA mismatch correction. Annu. Rev. Biochem. *56*, 435–466.

Natrajan, G., Lamers, M.H., Enzlin, J.H., Winterwerp, H.H., Perrakis, A., and Sixma, T.K. (2003). Structures of Escherichia coli DNA mismatch repair enzyme MutS in complex with different mismatches: a common recognition mode for diverse substrates. Nucleic Acids Res. *31*, 4814–4821.

Obmolova, G., Ban, C., Hsieh, P., and Yang, W. (2000). Crystal structure of *Taq* MutS and its complex with a heteroduplex DNA at 2.2Å resolution. Nature *407*, 703–710.

Painter, J., and Merritt, E.A. (2006). Optimal description of a protein structure in terms of multiple groups undergoing TLS motion. Acta Crystallogr. D Biol. Crystallogr. *62*, 439–450.

Peltomaki, P. (2003). Role of DNA mismatch repair defects in the pathogenesis of human cancer. J. Clin. Oncol. *21*, 1174–1179.

Rada, C., Ehrenstein, M.R., Neuberger, M.S., and Milstein, C. (1998). Hot spot focusing of somatic hypermutation in MSH2-deficient mice suggests two stages of mutational targeting. Immunity *9*, 135–141.

Rasmussen, L.J., and Samson, L. (1996). The *Escherichia coli* MutS DNA mismatch binding protein specifically binds O(6)-methylguanine DNA lesions. Carcinogenesis *17*, 2085–2088.

Samaranayake, M., Bujnicki, J.M., Carpenter, M., and Bhagwat, A.S. (2006). Evaluation of molecular models for the affinity maturation of antibodies: roles of cytosine deamination by AID and DNA repair. Chem. Rev. *106*, 700–719.

Schirmer, T., and Evans, P.R. (1990). Structural basis of the allosteric behaviour of phosphofructokinase. Nature *343*, 140–145.

Schofield, M.J., Nayak, S., Scott, T.H., Du, C., and Hsieh, P. (2001). Interaction of Escherichia coli MutS and MutL at a DNA mismatch. J. Biol. Chem. *276*, 28291–28299.

Stenson, P.D., Ball, E.V., Mort, M., Phillips, A.D., Shiel, J.A., Thomas, N.S., Abeysinghe, S., Krawczak, M., and Cooper, D.N. (2003). Human Gene Mutation Database (HGMD): 2003 update. Hum. Mutat. *21*, 577–581.

Stojic, L., Mojas, N., Cejka, P., Di Pietro, M., Ferrari, S., Marra, G., and Jiricny, J. (2004). Mismatch repair-dependent G2 checkpoint induced by low doses of SN1 type methylating agents requires the ATR kinase. Genes Dev. *18*, 1331–1344.

Studamire, B., Quach, T., and Alani, E. (1998). Saccharomyces cerevisiae Msh2p and Msh6p ATPase activities are both required during mismatch repair. Mol. Cell. Biol. *18*, 7590–7601.

Walker, J., Saraste, M., Runswick, M., and Gay, N. (1982). Distantly related sequences in the alpha- and beta-subunits of ATP synthase, myosin, kinases, and other ATP-requiring enzymes and a common nucleotide binding fold. EMBO J. *1*, 945–951.

Wallace, A.C., Laskowski, R.A., and Thornton, J.M. (1995). LIGPLOT: a program to generate schematic diagrams of protein-ligand interactions. Protein Eng. *8*, 127–134.

Wang, H., Yang, Y., Schofield, M.J., Du, C., Fridman, Y., Lee, S.D., Larson, E.D., Drummond, J.T., Alani, E., Hsieh, P., and Erie, D.A. (2003). DNA bending and unbending by MutS govern mismatch recognition and specificity. Proc. Natl. Acad. Sci. USA *100*, 14822–14827.

Warren, J.J., Forsberg, L.J., and Beese, L.S. (2006). The structural basis for the mutagenicity of O6-methyl-guanine lesions. Proc. Natl. Acad. Sci. USA *103*, 19701–19706.

Wilson, M.A., and Brunger, A.T. (2003). Domain flexibility in the 1.75 A resolution structure of Pb2+-calmodulin. Acta Crystallogr. D Biol. Crystallogr. *59*, 1782–1792.

Wilson, T.M., Vaisman, A., Martomo, S.A., Sullivan, P., Lan, L., Hanaoka, F., Yasui, A., Woodgate, R., and Gearhart, P.J. (2005). MSH2-MSH6 stimulates DNA polymerase eta, suggesting a role for A:T mutations in antibody genes. J. Exp. Med. *201*, 637–645.

Word, J.M., Lovell, S.C., LaBean, T.H., Taylor, H.C., Zalis, M.E., Presley, B.K., Richardson, J.S., and Richardson, D.C. (1999). Visualizing and quantifying molecular goodness-of-fit: small-probe contact dots with explicit hydrogen atoms. J. Mol. Biol. *285*, 1711–1733.

York, S.J., and Modrich, P. (2006). Mismatch repair-dependent iterative excision at irreparable O6-methylguanine lesions in human nuclear extracts. J. Biol. Chem. *281*, 22674–22683.

Yoshioka, K., Yoshioka, Y., and Hsieh, P. (2006). ATR kinase activation mediated by MutSalpha and MutLalpha in response to cytotoxic O6-methylguanine adducts. Mol. Cell *22*, 501–510.

## Accession Numbers

Structures have been deposited in the RCSB Protein Data Bank under PDB codes 2O8B, 2O8C, 2O8D, 2O8E, and 2O8F.